14th Australasian Fluid Mechanics Conference
Adelaide University, Adelaide, Australia
10-14 December 2001

Transverse Velocity and Temperature Derivative Measurements in Grid Turbulence

T. Zhou[1], R. A. Antonia[2], J-J. Lasserre[3] , M. Coantic[3] and F. Anselmet[3]

[1] School of Mechanical and Production Engineering
Nanyang Technological University, Singapore 639798
[2] Department of Mechanical Engineering
The University of Newcastle, NSW 2308, Australia
[3] I.R.P.H.E.
13453 Marseille Cedex 13, France

Abstract

The *same* probe, comprising two parallel wires, is used to measure either velocity or temperature derivatives in shearless grid turbulence. The aerodynamic interference of the probe affects the mean velocity when the transverse separation Δy between the wires is smaller than about 3η, where η ($\approx$0.4 mm) is the Kolmogorov length scale, but does not affect the mean temperature. Moments of transverse velocity and temperature derivatives are significantly but similarly affected when $\Delta y<3\eta$, thus suggesting that this effect is more likely to be caused by electronic noise than aerodynamic interference. After noise corrections are applied, the resulting derivative variances are brought into alignment with values inferred from two-point correlations with respect to y. Transverse derivative variances and their corresponding spectra satisfy isotropy closely but second-order structure functions satisfy it only when the separation is less than about 10η.

Introduction

The mean energy dissipation rate $\langle\varepsilon\rangle\equiv 2\nu\langle s_{ij}s_{ij}\rangle$ and the mean temperature variance dissipation rate $\langle\chi\rangle\equiv\kappa\langle\theta_{,i}\theta_{,i}\rangle$ are important quantities from theoretical as well as practical points of view, where $s_{ij}\equiv(u_{i,j}+u_{j,i})/2$ is the turbulent rate of strain, $u_{i,j}$ represents the velocity derivative $\partial u_i/\partial x_j$ and ν is the kinematic viscosity of the fluid; $\theta_{,i}$ represents the temperature derivative $\partial\theta/\partial x_i$ and κ is the thermal diffusivity of the fluid. Whilst a complete determination of ε and χ is possible in direct numerical simulations, experimentally, the task is fraught with difficulty since twelve velocity derivative and three temperature derivative correlations need to be determined simultaneously. The simplest way to approximate $\langle\varepsilon\rangle$ and $\langle\chi\rangle$ is by assuming isotropy, i.e.

$$\langle\varepsilon\rangle_{iso}=15\nu\langle(\partial u/\partial x)^2\rangle \qquad (1)$$

$$\langle\chi\rangle_{iso}=3\kappa\langle(\partial\theta/\partial x)^2\rangle, \qquad (2)$$

where u is the velocity component in the streamwise (x) direction and θ is the temperature fluctuation. It is generally assumed that $\partial u/\partial x$ and $\partial\theta/\partial x$ can be estimated from $\partial u/\partial t$ and $\partial\theta/\partial t$ using Taylor's hypothesis so that only single hot and cold wires are sufficient for determining $\langle\varepsilon\rangle_{iso}$ and $\langle\chi\rangle_{iso}$. Errors resulting from Taylor's hypothesis and the isotropic assumption cannot be discounted. The shortcomings of Taylor's hypothesis and local isotropy are relatively well known, especially in regions where local turbulence intensity is high and in the vicinity of walls. To measure all three components in χ, two orthogonal pairs of parallel cold wires are required (e.g. [1-3]). To measure all the twelve components involved in ε simultaneously, at least nine hot wires are needed (e.g. [4]). As the number of hot and cold wires increases, the spatial resolution of the probe becomes increasingly important [5,6]. In general, too large a measurement volume is likely to cause attenuation of the derivative spectra whereas noise contamination and possibly aerodynamic interference are expected to dominate as the measurement volume decreases.

The previous conflicting difficulties are best investigated in the context of a simple probe geometry, i.e. a pair of parallel wires (hot or cold). This arrangement has been analyzed by many investigators [2,6-8]. Recently, Lasserre [8] examined a wide range of possible causes for the spurious increase in the measured values of $\langle(\Delta u/\Delta y)^2\rangle$ and $\langle(\Delta\theta/\Delta y)^2\rangle$ as Δy decreases. Effects such as thermal and electrical cross-talk between the wires, differences between velocity sensitivities of the wires and uncertainty in estimating Δy were readily dismissed. Electronic noise was deemed to be important whilst aerodynamic disturbances due to the probe geometry could not be altogether eliminated. In the light of these observations, it was thought that more insight into the possible importance of the aerodynamic disturbance would be gained by using the *same* probe (same wires) and by operating the wires either as velocity sensors or as temperature sensors. In this way, the aerodynamic disturbance would be identical in each case so that the effects of reducing Δy on the spectra and variances of $\Delta u/\Delta y$ and $\Delta\theta/\Delta y$ can be assessed more meaningfully.

Experimental Details

Transverse velocity and temperature derivatives were measured in a wind tunnel at $x/M=30$ downstream of a grid, where x is measured from the grid and $M\equiv 24.76$ mm is the mesh size of the grid. The Taylor microscale Reynolds number R_λ is 40 [$R_\lambda\equiv u'\lambda/\nu$, the prime denotes rms value and $\lambda\equiv u'/\langle(\partial u/\partial x)'\rangle$ is the longitudinal Taylor microscale]. The main reason for selecting such a low R_λ is that, at this speed, the Kolmogorov frequency f_K ($\equiv U/2\pi\eta$, where $\eta\equiv\nu^{3/4}/\langle\varepsilon\rangle^{1/4}$ is the Kolmogorov length scale) is about 1550 Hz. This is close to the 3dB cut-off frequency of the wires when operated in constant current mode, thus minimizing errors caused by high frequency noise. The grid, located at the entrance of the working section, has a square mesh with a solidity of 35%. A *mandoline*, located a distance of 1.5M downstream of the grid, was used for introducing heat into the flow. Details of the *mandoline* can be found in [9]. The probe consists of two parallel wires with separation $\Delta y^*=0.5$-15. The asterisk denotes normalization by η, the velocity scale $u_K\equiv(\nu/\langle\varepsilon\rangle)^{1/2}$ and/or the

temperature scale $\theta_K \equiv (<\chi>\eta/u_K)^{1/2}$. The wire prongs were inclined to about 45° to the *x*-axis in an attempt to "minimize" the aerodynamic disturbance, since according to Comte-Bellot et al. [10], an inclination of either 0° or 90° would tend to maximize the disturbance. The wires had a diameter of 1.27μm and were etched from Wollaston (Pt-10% Rh) wire to an active length of about 0.8mm. The output signals from the anemometers were passed through buck and gain circuits and low-pass filtered at a cut-off frequency f_c=1250 Hz. The signal-to-noise (SN) ratio was estimated to be about 200 for the hot wires and about 50 for the cold wires.

Experimental Results

The effect of Δy on the mean velocity U and temperature *T* is shown in Figure 1. The mean velocity distributions from wires 1 and 2 remain within ±0.5% of the averaged value of the two wires for $\Delta y^*>3.0$. It would appear that there is no aerodynamic interference effect on U for this Δy range. As Δy^* decreases below 3.0, *U* from wire 1 increases whereas *U* from wire 2 decreases. The effect on *U* for $\Delta y^*<3.0$ is not due to cross-talk between the wires since varying the overheat of one of the wires did not affect either of the distributions of *U* in Figure 1 (for a detailed study of the cross-talk effect, see [8]). The two distributions of *T* follow each other closely and remain within ±0.5% of their average value, independently of Δy. Given that the experimental uncertainty in measuring *T* is about ±1%, it seems reasonable to conclude that, any aerodynamic interference due to the geometry of the probe does not affect the mean temperature sensed by the wires.

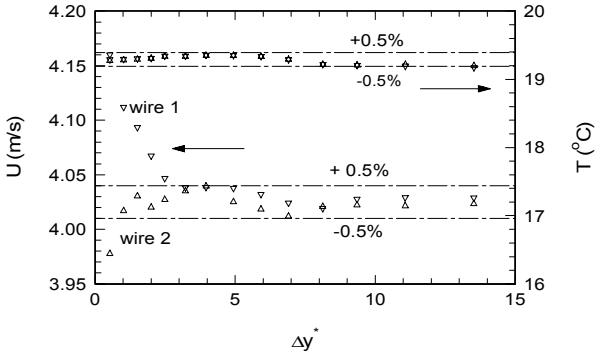

Figure 1. Mean velocity and mean temperature for different wire separations. Δ: wire 1; ∇: wire 2. The dot-dashed lines correspond to ±0.5% of the averaged values of wires 1 and 2.

The effect of Δy on u' and θ' is shown in Figure 2. To within the experimental uncertainty (±2%), u' and θ' can be considered to be independent of Δy, implying the absence of any aerodynamic effect on the fluctuating signals. Further corroboration of this is provided by the spectra of u and θ in Figure 3. Here, the spectral density $\phi_\alpha(k_1)$ is defined such that $\int_0^\infty \phi_\alpha(k_1)dk_1 = <\alpha^2>$. There is nearly no difference between $\phi_u(k_1)$ [or $\phi_\theta(k_1)$] for different separations, independently of the wavenumber. To avoid crowding, only spectra corresponding to two different wire separations are shown in Figure 3.

The values of $<(\Delta u^*/\Delta y^*)^2>$ and $<(\Delta\theta^*/\Delta y^*)^2>$ for different wire separations are shown in Figure 4. For isotropic turbulence, $<(\partial u^*/\partial y^*)^2>$ and $<(\partial\theta^*/\partial y^*)^2>$ should be 2/15 and Pr/3 (≈0.24) respectively. It is expected that $<(\partial u^*/\partial y^*)^2>$ and $<(\partial\theta^*/\partial y^*)^2>$ are approached monotonically by $<(\Delta u^*/\Delta y^*)^2>$ and $<(\Delta\theta^*/\Delta y^*)^2>$ in the limit of $\Delta y^*\to 0$. However, the trend shown in Figure 4 indicates that $<(\Delta u^*/\Delta y^*)^2>$ and $<(\Delta\theta^*/\Delta y^*)^2>$ increase systematically in a rapid and spurious manner. The sharp increase of $<(\Delta u^*/\Delta y^*)^2>$ and $<(\Delta\theta^*/\Delta y^*)^2>$ has been assumed (e.g. [2,6]) to reflect mainly the noise contamination but Mestayer and Chambaud [5] also considered the contribution from errors in wire calibration. The decrease of $<(\Delta u^*/\Delta y^*)^2>$ and $<(\Delta\theta^*/\Delta y^*)^2>$ at larger Δy^* reflects the impairment in spatial resolution. Figure 4 indicates that there is only a small range (e.g. Δy^*=4-5) over which $<(\Delta u^*/\Delta y^*)^2>$ and $<(\Delta\theta^*/\Delta y^*)^2>$ agree favorably with their corresponding isotropic values.

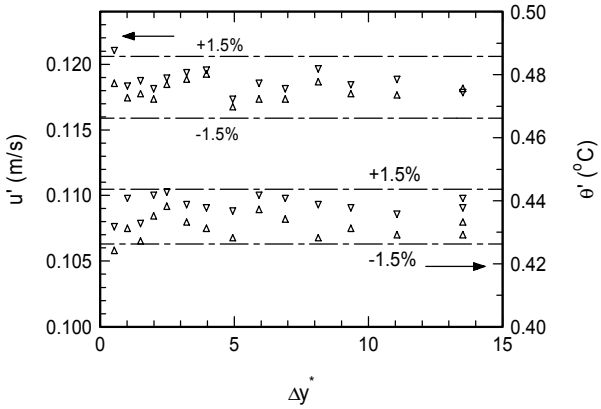

Figure 2. Rms values of velocity and temperature fluctuations for different wire separations. Δ: wire 1; ∇: wire 2. The dot-dashed lines correspond to ±1.5% of the averaged values of wires 1 and 2.

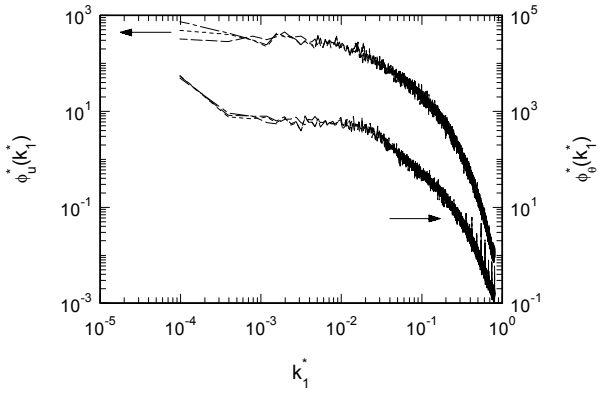

Figure 3. Velocity and temperature spectra for different wire separations. – –: Δy^*=0.5 (from wire 1); — - —: Δy^*=0.5 (from wire 2); — —: Δy^*=13.5.

The correction for noise contamination can be made using a method similar to that outlined in [2]. These corrected values are also included in Figure 4. The resulting variations of $<(\Delta u^*/\Delta y^*)^2>$ and $<(\Delta\theta^*/\Delta y^*)^2>$ with respect to Δy^* are clearly smaller than those of the original (noise contaminated) values.

The values of the derivative variances $<(\partial u^*/\partial y^*)^2>$ and $<(\partial\theta^*/\partial y^*)^2>$ can also be inferred from the correlations between u(y) and u(y+Δy) or between θ(y) and θ(y+Δy). Using Taylor series expansions, to order $(\Delta y)^3$, the auto correlation coefficients of u and θ can be written as:

$$\rho_u = 1 - \frac{(\Delta y)^2}{2<u^2>}<(\partial u/\partial x)^2> + \vartheta\left[(\Delta y)^3\right] \qquad (3)$$

$$\rho_\theta = 1 - \frac{(\Delta y)^2}{2 < \theta^2 >} < (\partial\theta / \partial x)^2 > + \vartheta\left[(\Delta y)^3\right]. \qquad (4)$$

Parabolic fits to the distributions of ρ_u and ρ_θ yielded the values of $<(\partial u^*/\partial y^*)^2>$ and $<(\partial\theta^*/\partial y^*)^2>$ (indicated by horizontal arrows next to the vertical axes) in Figure 4. These values are in close agreement with the peaks of the noise-corrected distributions of $<(\Delta u^*/\Delta y^*)^2>$ and $<(\Delta\theta^*/\Delta y^*)^2>$. Note that the values of ρ_u and ρ_θ were noise-corrected; although the correlations are unaffected by noise, the correlation coefficients are affected through the variances of u and θ.

The spectra of $\Delta u^*/\Delta y^*$ and $\Delta\theta^*/\Delta y^*$ have been corrected for the attenuation caused by the finite values of Δy and the effect of wire length *l*. Details of the correction procedures can be found in Antonia and Mi [11]. The corrected values of $<(\Delta u^*/\Delta y^*)^2>$ and $<(\Delta\theta^*/\Delta y^*)^2>$, which are also included in Figure 4, were estimated by integrating the corrected spectra of $\Delta u^*/\Delta y^*$ and $\Delta\theta^*/\Delta y^*$. They are essentially constant and agree to within ±0.5% with the corresponding isotropic values for $\Delta y^* \geq 8$. When Δy^* decreases, the corrected values of $<(\Delta u^*/\Delta y^*)^2>$ and $<(\Delta\theta^*/\Delta y^*)^2>$ increase slightly. At $\Delta y^* = 4$, the magnitudes of $<(\Delta u^*/\Delta y^*)^2>$ and $<(\Delta\theta^*/\Delta y^*)^2>$ are about 10% and 15% greater than the derivative values inferred from the correlations. It is likely that this discrepancy reflects the fact that the spectra for $\Delta u^*/\Delta y^*$ and $\Delta\theta^*/\Delta y^*$ have not been corrected for noise contamination. Such a correction would have required recordings of unfiltered signals ([8]), which, unfortunately, were not made, as well as a basis for extrapolating the noise spectrum to lower frequencies.

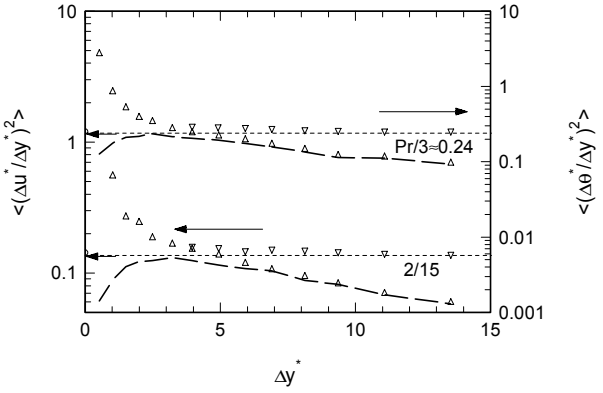

Figure 4. Dependence of $<(\Delta u^*/\Delta y^*)^2>$ and $<(\Delta\theta^*/\Delta y^*)^2>$ on wire separation. Δ: measured; ∇: spectrally corrected; – –: isotropic values; — —: noise-corrected. o on the ordinate: $2<(\partial u^*/\partial x^*)^2>$ or $<(\partial\theta^*/\partial x^*)^2>$. Horizontal arrows next to the vertical axes indicate $<(\Delta u^*/\Delta y^*)^2>$ and $<(\Delta\theta^*/\Delta y^*)^2>$ obtained from Eqs. (3) and (4).

The measurements of Δu/Δy and Δθ/Δy allow several isotropy checks to be made. One measure of departure from isotropy is provided by comparing the measured spectra with calculations using isotropic relations (e.g. [12])

$$\phi^{cal}_{\partial\alpha/\partial y} = 2\int_{k_1}^{\infty} \frac{1}{k}\phi_{\partial\alpha/\partial x}(k_1)dk \qquad (5)$$

where the superscript *cal* denotes "calculation" and α represents either u or θ. Comparisons between measured and calculated distributions of $\phi_{\partial u/\partial y}$ and $\phi_{\partial\theta/\partial y}$ for $\Delta y^* = 4$ are shown in Figure 5. In each case, there is a significant wavenumber range over which the agreement between the two distributions may be tolerable. When the ratio $\phi^{cal}_{\partial\alpha/\partial y}/\phi_{\partial\alpha/\partial y}$ is plotted on a linear scale, its magnitude remains within 10% of 1 (the isotropic value) over the range $k_1^* < 0.6$ except for $\alpha = \theta$ at $k_1^* \leq 0.003$.

For isotropic turbulence, the second-order longitudinal and transverse velocity structure functions are related by (e.g. [12])

$$< (\delta S_T)^2 >= \left[1 + \frac{\Delta x}{2}\frac{\partial}{\partial(\Delta x)}\right] < (\delta S_L)^2 > \qquad (6)$$

where δS_L is the longitudinal velocity structure function which can be obtained from the longitudinal velocity fluctuations by converting the time delay τ to a spatial increment Δx (≡Uτ) using Taylor's hypothesis, i.e. $\delta S_L = u(x+\Delta x) - u(x)$. The transverse structure function δS_T can be obtained either from two-point longitudinal velocity measurements separated by a transverse distance Δy, i.e. $\delta S_T = u(y+\Delta y) - u(y)$ or from one-point measurements of the transverse velocity component separated by a longitudinal distance, i.e. $\delta S_T = v(x+\Delta x) - v(x)$. In Figure 6, the measured values of $<[\Delta u(\Delta y)]^2>$ and $<[\Delta v(\Delta x)]^2>$ are compared with those calculated using Eq. (6) based on the measured values of $<(\delta S_L)^2>$. Because of the relatively poor temporal resolution of the data at small values of Δx, an interpolation formula (e.g. [13]) was first fitted (dotted line) to the measured values of $<[\Delta u(\Delta x)]^2>$ before carrying the differentiation with respect to Δx as per Eq. (6). The resulting distribution of calculated $<(\delta S_T)^2>$ follows the measurements of $<[\Delta u(\Delta y)]^2>$ for $\Delta y^* \leq 10$, indicating that isotropy is approximately satisfied only for scales within the dissipative range. In the limit $\Delta y^* \to 0$, the second-order structure functions must vary as $(\Delta y^*)^2$; a line of slope 2 has been included to show that this is indeed the case.

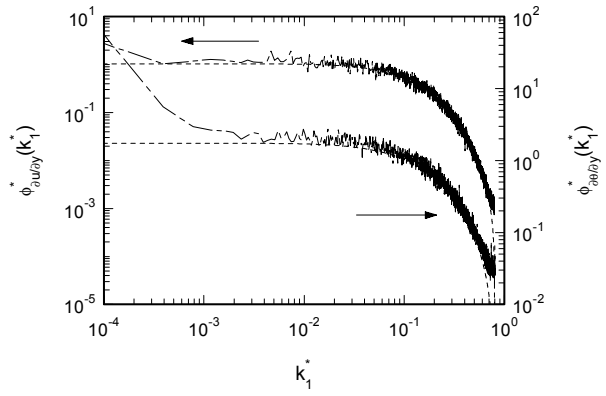

Figure 5. Comparison between measured and calculated [Eq. (5)] transverse velocity and temperature derivative spectra.
- - -: Calculated; — - —: measured.

In isotropic turbulence, the second-order scalar structure functions should be independent of the direction in which the separation is taken (e.g. [14]), i.e.

$$< [\Delta\theta(\Delta y)]^2 >=< [\Delta\theta(\Delta x)]^2 > \qquad (7)$$

This relation has been checked by [14] in a heated turbulent boundary layer and by Mydlarski and Warhaft [15] in slightly heated turbulence downstream of an active grid with a mean temperature gradient. Mestayer [14] found that Eq. (7) was not satisfied, either in the scaling range or in the dissipative range. On

the other hand, Mydlarski and Warhaft [15] verified (7) in the inertial range whilst, in the dissipative range, the left side of (7) is about 50% larger than the right side, independently of R_λ. This latter result violates isotropy. The present distributions of $<[\Delta\theta(\Delta y)]^2>$ and $<[\Delta\theta(\Delta x)]^2>$ are shown in Figure 7. They satisfy (7) reasonably well for Δx^* (or Δy^*) ≤ 10; as expected, at small Δy^*, $<[\Delta\theta(\Delta y)]^2>$ varies as Δy^{*2} to a good approximation. The previous results may reflect an important difference between the present flow, in which the scalar variance is spatially decaying, and the flows considered by [14] and [15], where mean temperature gradients were present, thus providing a continuous supply of $<\theta^2>$. Collectively, Figures 6 and 7 suggest that strictly only the smallest scales (that fall within the dissipative range) satisfy isotropy in the present low Reynolds number grid turbulence. This small range of scales is not easily reconcilable with the relatively large wavenumber range over which measured velocity and temperature derivative spectra agree with corresponding isotropic calculations (Figure 5). This difference suggests that the translation between the power-law range in the energy or temperature spectrum (i.e. the spectral domain) and that in the structure function (i.e. the physical domain) is inexact, as was discussed in detail by Hou et al. [16]. Consequently, the ranges over which local isotropy is satisfied in the physical and spectral domains are unlikely to be identical, especially when R_λ is small.

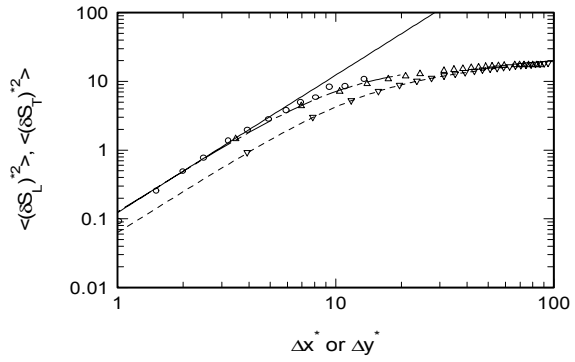

Figure 6. Comparison of measured second-order transverse structure functions with isotropic calculations. The solid line has a slope of 2.
∇: $<[\Delta u(\Delta x)]^2>$; Δ: $<[\Delta v(\Delta x)]^2>$; o: $<[\Delta u(\Delta y)]^2>$; — - —: $<(\delta S_T)^2>$ from Eq. (6); – –: fit to $<[\Delta u(\Delta x)]^2>$.

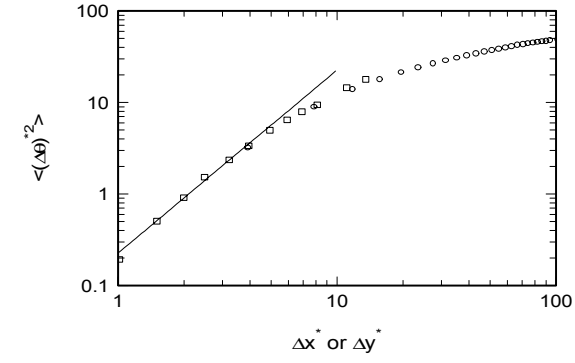

Figure 7. Comparison between temperature structure functions obtained with separations in x and y directions. The solid line has a slope of 2.
O: $<[\Delta\theta(\Delta x)]^2>$; □ : $<[\Delta\theta(\Delta y)]^2>$.

Conclusions

The present measurement results indicate that the mean velocity *U* measured by the two wires is not influenced by the transverse separation between the wires unless Δy is smaller than about 3η. As expected, this interference does not influence the mean temperature T. Perhaps surprisingly, there is no discernible effect of Δy on either the rms velocity or rms temperature values. The noise corrected values of $<(\Delta u^*/\Delta y^*)^2>$ and $<(\Delta\theta^*/\Delta y^*)^2>$ can be reconciled both with the derivative variances inferred from the two-point correlation functions, with respect to *y*, of *u* and θ and the longitudinal derivative variances $2<(\partial u/\partial x)^2>$ and $<(\partial\theta/\partial x)^2>$. Second-order velocity and temperature structure functions indicate that only dissipative scales ($\Delta y^* \le 10$) satisfy isotropy. This range is much smaller than that for which the spectra of $\partial u/\partial y$ and $\partial\theta/\partial y$ satisfy isotropy.

Acknowledgement

RAA gratefully acknowledges the support of the Australian Research Council.

References

[1] Sreenivasan, K. S., Antonia, R. A. and Danh, H. Q., Temperature dissipation fluctuations in a turbulent boundary layer, *Phys. Fluids*, **20**, 1977, 1238-1249.

[2] Anselmet, F., Djeridi, H. and Fulachier, L., Joint statistics of a passive scalar and its dissipation in turbulent flows, *J. Fluid Mech*. **280**, 1994, 173-197.

[3] Danaila, L., Zhou, T., Anselmet, F. and Antonia, R. A., Calibration of a temperature dissipation probe in decaying grid turbulence, *Expts. in Fluids*, **28**, 2000, 45-50.

[4] Wallace, J. M. and Foss, J. F., The measurement of vorticity in turbulent flows, *Ann. Rev. Fluid Mech*., **27**, 1995, 467-514.

[5] Mestayer, P. and Chambaud, P., Some limitations to measurements of turbulence micro-structure with hot and cold wires, *Boundary-Layer Meteorol*., **19**, 1979, 311-329.

[6] Antonia, R. A., Browne, L. W. B. and Chambers, A. J., On the spectrum of the transverse derivatives of the streamwise velocity in a turbulent flow, *Phys. Fluids*, **27**, 1984, 2628-2631.

[7] Wyngaard, J. C., Spatial resolution of the vorticity meter and other hot wire arrays, *J. Sci. Instrum*., **2**, 1969, 983-987.

[8] Lasserre, J-J., Méthodes pratiques de détermination du taux de dissipation de l'énergie cinétique de la turbulence par anémométrie à fils chauds, Thèse de Docteur de l'Université Aix-Marseille II, 2000.

[9] Zhou, T. and Antoina, R. A., Approximation for turbulent energy and temperature dissipation rates in grid turbulence, *Phys. Fluids*, **12**, 2000, 335-344.

[10] Comte-Bellot, G., Strohl, A. and Alcaraz, E., On aerodynamic isturbances caused by single hot-wire probes*, J. Appl. Mech*., **38**, 1971, 767-774.

[11] Antonia, R. A. and Mi, J., Corrections for velocity and temperature derivatives in turbulent flows, *Expts. in Fluids*, **14**, 1993, 203-208.

[12] Monin, A. S. and Yaglom, A. M., *Statistical Fluid Mechanics*, **Vol. 2**, MIT Press, 1975.

[13] Batchelor, G. K., Pressure fluctuations in isotropic turbulence, *Proc. Cambridge Philos. Soc*. **47**, 1951, 359-374.

[14] Mestayer, P., Local isotropy and anisotropy in a high-Reynolds-number turbulent boundary layer, *J. Fluid Mech*., **125**, 1982, 475-503.

[15] Mydlarski, L. and Warhaft, Z., Passive scalar statistics in high-Peclet-number grid turbulence, *J. Fluid Mech*., **358**, 1998, 135-175

[16] Hou, Y., Wu, X-H, Chen. S. and Zhou, Y., Effect of finite computational domain on turbulence scaling law in both physical and spectral spaces, *Phys. Rev. E*, **58**, 1998, 5841-5844.